IEEE Access
Multidisciplinary | Rapid Review | Open Access Journal

Received December 11, 2018, accepted December 31, 2018, date of publication February 7, 2019, date of current version February 20, 2019.

Digital Object Identifier 10.1109/ACCESS.2019.2892080

Impedance Shaping of Isolated Two-Stage AC-DC-DC Converter for Stability Improvement

FAN FENG[1], FENGJIANG WU[2], (Senior Member, IEEE), AND HOAY BENG GOOI[1], (Senior Member, IEEE)

[1]School of Electrical and Electronic Engineering, Nanyang Technological University, Singapore 639798
[2]Department of Electrical Engineering, Harbin Institute of Technology, Harbin 150001, China

Corresponding author: Fengjiang Wu (shimeng@hit.edu.cn)

This work was supported by the Energy Innovation Programme Office through the National Research Foundation and Singapore Energy Market Authority under Project LA/Contract NRF2014EWT-EIRP002-005.

ABSTRACT The isolated two-stage ac–dc–dc converter containing an isolated dual-active-bridge (DAB) dc–dc converter and an ac–dc rectifier has been widely used for connecting the dc sources to the ac utility grid. However, the impedance interaction between the DAB converter and the ac–dc rectifier may cause the instability problem. To address this issue, this paper proposes two control methods to reshape the impedances of the isolated two-stage ac–dc–dc converter by building a virtual impedance connected in parallel or series with the input impedance of the DAB converter. The magnitude of the input impedance of the DAB converter is increased to satisfy the Middlebrook criterion without changing its negative resistance characteristics by the proposed control methods. Furthermore, the design requirements for the proposed controllers are also given to ensure the stable operation of the two-stage converter. The comparison of these two proposed methods is also discussed in terms of stabilizing ability, dynamic performance, and cost. The comprehensive experimental results are provided to validate the proposed methods.

INDEX TERMS Impedance shaping, modeling, stability criterion, two-stage converter.

I. INTRODUCTION

Integration of various DC energy sources, such as batteries and PV panels, to the AC utility grid brings benefits to the sustainability and efficiency of the modern utility grid [1], [2]. One of the typical connections between the DC source and AC grid is the bidirectional two-stage AC-DC-DC converter. For the DC-DC conversion stage, dual active bridge (DAB) converters are attracting more and more attention because of its advantages such as the bidirectional power flow, high power density and galvanic isolation. Hence, the DAB-based two-stage converter shown in Fig. 1 has been widely used as the interface between the DC sources and AC grid [3]–[6].

Despite the above merits, the DAB-based two-stage converter suffers from unstable problems. Similar instability issues have also been reported in [7]–[9]. The stability criteria for unidirectional two-stage converters have been proposed in [10]–[12]. The two-stage converter is stable only if the impedances of the source and load converters satisfy the Middlebrook impedance ratio stability criterion. However, in bidirectional applications, the role of source/load converter can be changing dynamically. It has been found that the stability of the bidirectional two-stage converter is related to its control strategy. When the power is transferred from the voltage controlled sub-converter to the current controlled sub-converter, the bidirectional two-stage converter may be unstable [9].

In order to meet the impedance-based stability criterion in the two-stage converter and other cascaded systems, several techniques have been proposed to reshape the source output or the load input impedance. Basically, they can be divided into two categories: passive methods and active methods. For the passive methods, the passive components, typically a resistor and a capacitor are added in parallel with the DC-link filter to reduce the source converter's impedance [13]–[15]. However, the resistance leads to an additional cost and power loss. Moreover, the large electrolytic capacitance is undesirable in the high-reliability applications due to its short lifetime expectancy [16], [17].

As an alternative, the active methods based on the advanced control are proposed to improve the stability of the two-stage converter [18]–[20]. A buffer converter is applied between the source and load to modify the impedance interaction

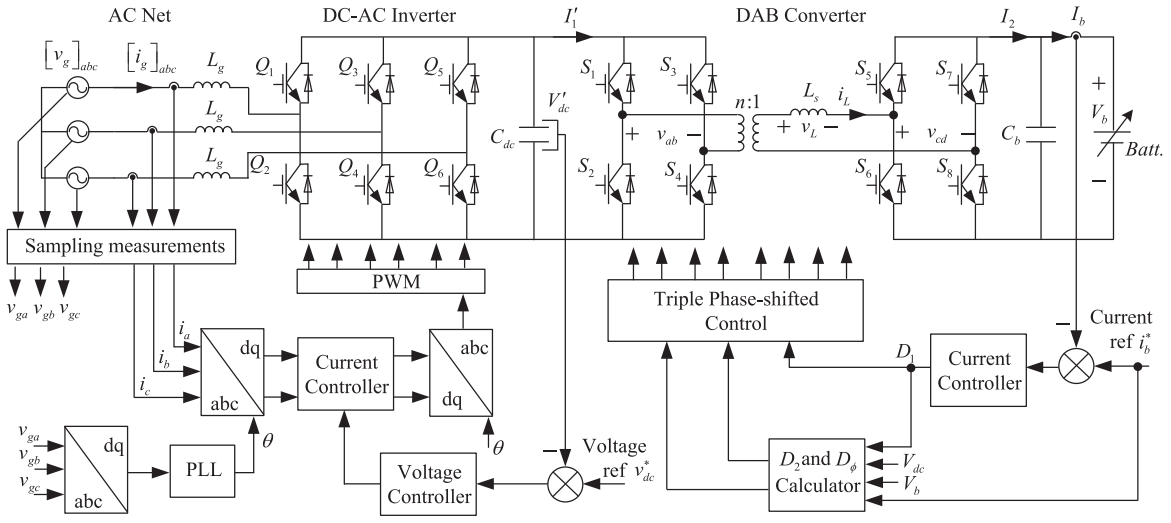

FIGURE 1. Topology and closed-loop control configuration of the two-stage AC-DC-DC converter.

in [21] and [22]. However, this approach needs to redesign the main circuit, which is time-consuming especially for the modularly designed circuits. The output impedance of the source converter can be decreased by the active damping methods proposed in [23] and [24]. As a result, the two-stage converters can satisfy the impedance-based stability criterion. But these methods are effective only in the two-stage power converter applications. They are not suitable for solving the instability problems between the power converters and their *LC* input filters, as the output impedance of the *LC* filter is unchangeable. In [25]–[28], an active controller is applied to reshape the input impedance of the load converter. The phase of the load converter's input impedance is compensated to be positive by adding a virtual resistor or capacitor to the load converter. It is because the negative resistive input impedances of the load converters are threats for the stability. Hence, the stability of the two-stage converter can be successfully improved by these impedance shaping methods [29], [30]. However, the input impedance of the load converter should be negative resistance to achieve good dynamics [31]. Therefore, it is challenging to reshape the input impedance of the load converter without affecting its dynamic performance. Moreover, the above-mentioned impedance shaping methods have not been applied to the isolated DAB-based two-stage systems yet. The AC characteristics of the inductor current bring the difficulties for the impedance modeling of the DAB converter.

This paper proposes two impedance shaping methods to improve the stability of the isolated DAB-based two-stage converter. In the proposed impedance shaping methods, the input impedance of the DAB converter is modified to satisfy the stability criterion without changing its negative resistance characteristics. In addition, the proposed methods mainly focus on modifying the impedance within the low frequency range, which greatly reduces the influence on the dynamic performances of the two-stage converter.

The rest of the paper is organized as follows. The impedance model of the DAB-based two-stage converter is recapped in section II. Two active stabilization methods are proposed to improve the stability of the two-stage converter and the controller design rules are elaborated in section III. The experimental results are provided to verify the proposed methods in section IV. The conclusion is given in section V.

II. SMALL SIGNAL IMPEDANCE MODELING OF TWO-STAGE AC-DC-DC CONVERTER

From Fig. 1, the control of the two-stage AC-DC-DC converter can be split into two parts in this paper: the DAB based DC-DC conversion stage and the AC-DC inversion stage. The DAB converter is tasked to regulate the battery current I_b. The AC-DC rectifier is responsible for maintaining the DC-link voltage constant and realizing the grid current control. Considering the stability strategy, the impedances of the two-stage converter are derived in the following subsections for stability analysis.

A. IMPEDANCE MODELING OF DAB CONVERTER

The simplified circuit of the DAB converter shown in Fig. 2 is used for the derivation of the small signal model. All the power switches are considered as ideal switches. I_b and V_b are the battery current and voltage, respectively. For the sake of simplification, the output of AC-DC rectifier is regarded as an ideal DC source, denoted as V'_{dc} in Fig. 2.

To eliminate the dual-DC-side circulating currents of the DAB converter, we have proposed the cooperative triple-phase-shift (CTPS) control method [32], [33], which is also used in this paper to control the DAB converter. The operation waveforms of this control are shown in Fig. 3, where I_1 and v_{ab} are used to denote I'_1 and v'_{ab} reflected to the secondary side of the transformer. d_1 and d_2 are the inner phase-shifts of the primary and secondary H-bridges, respectively. d_φ is the outer phase-shift between v_{ab} and v_{cd}. The relationship of

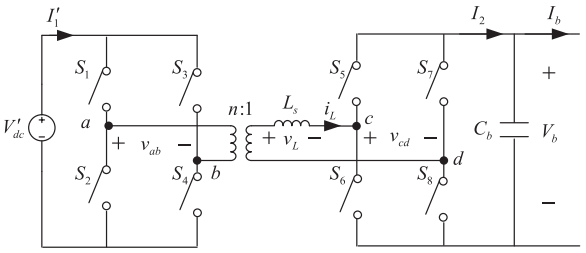

FIGURE 2. Simplified circuit diagram of the DAB converter.

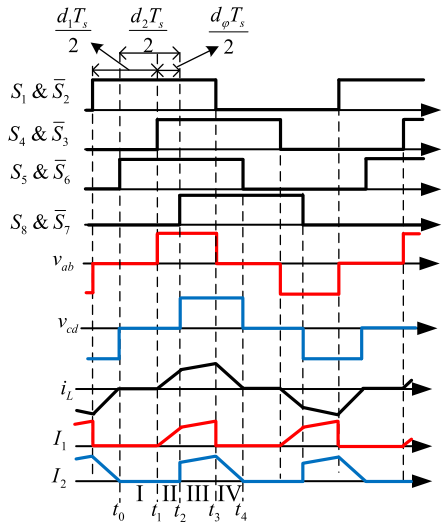

FIGURE 3. Operating waveforms of the CTPS-based DAB converter.

the three phase-shifts is expressed as:

$$d_2 = d_\varphi = 1 + k\,(d_1 - 1) \tag{1}$$

where $k = V_{dc}/V_b$; n is the turns ratio of the transformer; $V_{dc} = V_{dc}'/n$ is the DC-link voltage reflected to the secondary side; andT_s is the switching period.

As I_1 equals to i_L during the periods II and III, the average value of input current I_{1_av} can be expressed as (2). Similarly, the DAB output current I_2 equals to i_L during the periods III and IV. Hence, the average value of I_{2_av} is shown in (3).

$$I_{1_{av}} = \frac{T_s}{4L_s}\left[V_{dc}d_\varphi\,(1-d_1) + V_o d_1\left(1-d_1-d_\varphi\right)\right] \tag{2}$$

$$I_{2_{av}} = \frac{T_s}{4L_s}\left[V_{dc}d_\varphi\left(1-d_1-d_\varphi\right) + V_o d_1\left(1-d_\varphi\right)\right] \tag{3}$$

Applying the small signal perturbation to (2) and (3), the small signal model of the input and output current can be represented by (4) and (5), where the capital variables represent the steady state values and $\hat{x}$ represents the small signal variables of x. These rules apply to the entire paper.

$$\hat{i}_1 = \frac{T_s}{4L_s}\left\{\begin{array}{l}\left(1-2D_1-D_\varphi\right)V_b\hat{d}_1 + \left(1-D_1-2D_\varphi\right)V_b\hat{d}_\varphi \\ +\left[\left(1-D_\varphi\right)D_\varphi + \left(1-D_1-D_\varphi\right)D_1\right]\hat{v}_b\end{array}\right\} \tag{4}$$

$$\hat{i}_2 = \frac{T_s}{4L_s}\left\{\begin{array}{l}\left(1-2D_1-D_\varphi\right)V_{dc}\hat{d}_1 + \left(1-D_1-2D_\varphi\right)V_{dc}\hat{d}_\varphi \\ +\left[\left(1-D_1-D_\varphi\right)D_\varphi + \left(1-D_1\right)D_1\right]\hat{v}_{dc}\end{array}\right\} \tag{5}$$

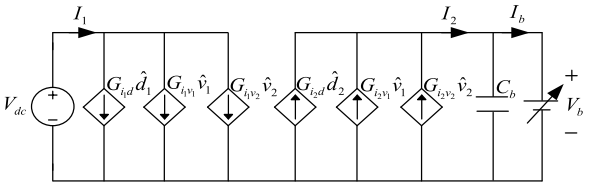

FIGURE 4. Small signal model of the DAB converter.

After linearizing (1), $\hat{d}_\varphi$ can be expressed as (6).

$$\hat{d}_\varphi = \frac{V_{dc}}{V_b}\hat{d}_1 + \frac{D_1-1}{V_b}\hat{v}_{dc} - \frac{D_\varphi - 1}{V_b}\hat{v}_b \tag{6}$$

Substituting (6) into (4) and (5), the open-loop small signal model of the DAB converter can be obtained as (7) and (7), where $G_{i_1d_1}$, $G_{i_1v_{dc}}$ and $G_{i_1v_b}$ are the transfer functions from $\hat{d}_1$, $\hat{v}_{dc}$ and $\hat{v}_b$ to $\hat{i}_1$ respectively. $G_{i_2d_1}$, $G_{i_2v_{dc}}$ and $G_{i_2v_b}$ are the transfer functions from $\hat{d}_1$, $\hat{v}_{dc}$ and $\hat{v}_b$ to $\hat{i}_2$ respectively.

$$\hat{i}_1 = G_{i_1d_1}\hat{d}_1 + G_{i_1v_{dc}}\hat{v}_{dc} + G_{i_1v_b}\hat{v}_b \tag{7}$$

$$G_{i_1d_1} = \frac{T_s}{4L_s}\left[\left(1-2D_1-D_\varphi\right)V_b + \left(1-D_1-2D_\varphi\right)V_{dc}\right] \tag{7.a}$$

$$G_{i_1v_{dc}} = \frac{T_s}{4L_s}\left[\left(1-D_\varphi\right)^2 - D_1^2\right] \tag{7.b}$$

$$G_{i_1v_b} = \frac{T_s}{4L_s}\left(1-D_1-2D_\varphi\right)(D_1-1) \tag{7.c}$$

$$\hat{i}_2 = G_{i_2d_1}\hat{d}_1 + G_{i_2v_{dc}}\hat{v}_{dc} + G_{i_2v_b}\hat{v}_b \tag{8}$$

$$G_{i_1d_1} = \frac{T_s}{2L_s}\left[\left(1-D_1-D_\varphi\right)V_{dc} - D_\varphi\frac{V_{dc}^2}{V_b}\right] \tag{8.a}$$

$$G_{i_2v_{dc}} = \frac{T_s}{4L_s}\left[(D_1-1)\left(1-D_1-2D_\varphi\right) - 3D_\varphi^2 + 2D_\varphi\right] \tag{8.b}$$

$$G_{i_2v_b} = \frac{T_s}{4L_s}\left[\left(1-D_\varphi\right)^2 + 2D_\varphi\left(D_\varphi-1\right)\frac{V_{dc}}{V_b}\right] \tag{8.c}$$

Based on (7) and (7), the complete small signal circuit of the CTPS-based DAB converter can be shown in Fig. 4. The small signal of the battery current I_b can be expressed as

$$\hat{i}_b\,(s) = \hat{i}_2\,(s) - C_b s\hat{v}_b \tag{9}$$

The control block diagram of the CTPS-based DAB converter is illustrated in Fig. 5, where $G_{ci} = K_p + K_i/s$ is the current controller. The input admittance Y_{in_DAB} of the DAB converter is expressed as (10). The input impedance Z_{in_DAB} of the DAB converter can be obtained as (11).

$$Y_{in\_DAB} = \frac{\hat{i}_1}{\hat{v}_{dc}} = G_{i_1v_1} - \frac{G_{i_1d_1}G_{ci}G_{i_2v_1}}{1+G_{ci}G_{i_2d_1}} \tag{10}$$

$$Z_{in\_DAB} = \frac{1+G_{ci}G_{i_2d_1}}{G_{i_1v_1} + G_{i_1v_1}G_{ci}G_{i_2d_1} - G_{i_1d_1}G_{ci}G_{i_2v_1}} \tag{11}$$

B. IMPEDANCE MODELING OF AC-DC RECTIFIER

From Fig. 1, the control of the AC-DC rectifier is implemented in the d-q frame. The grid voltage is measured by the phase-locked loop to synchronize the AC-DC rectifier

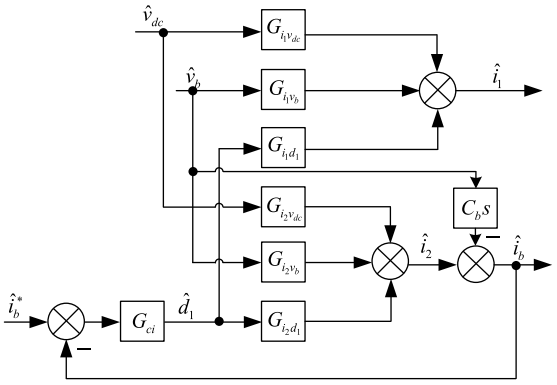

FIGURE 5. Control block diagram of the DAB converter.

operation. The grid current is regulated by the inner current control loop, while the outer control loop maintains the DC-link voltage constant. $G_{acv} = K_{pv} + K_{iv}/s$ and $G_{aci} = K_{pi}+K_{ii}/s$ are the voltage and current controller of the AC-DC rectifier, respectively. The small signal model of the AC-DC rectifier is shown in (12) with more details of derivation found in [34]. ω_1 is the angular frequency of the rectifier. i_d and i_q denote the d- and q-axes components of the grid current, respectively. D_d and D_q denote the d- and q-axes components of the duty ratio of the AC-DC rectifier, respectively (12), as shown at the bottom of this page.

Based on the closed-loop small signal model, the output impedance Z_{out} of the AC-DC rectifier is calculated in (13). A_c is the system matrix of (12).

$$Z_{out} = \frac{1}{|sI - A_c|}\frac{1}{C_{dc}}\left[(s + \frac{V_{dc}G_{ci}}{L_g})^2 + \omega_1^2\right] \tag{13}$$

III. PROPOSED IMPEDANCE SHAPING METHODS FOR STABILIZATION OF TWO-STAGE CONVERTER

A. STABILITY ANALYSIS OF TWO-STAGE CONVERTER

The stability of the two-stage converter can be determined by the impedance-based stability criterion. If the source converter is voltage controlled, the impedance ratio T_m is expressed as $T_m = Z_{out\_S}/Z_{in\_L}$, where Z_{out_S} is the output impedance of the source converter and Z_{in_L} is the input impedance of the load converter. If the source converter is current controlled, T_m is organized as $T_m = Z_{in\_L}/Z_{out\_S}$. If T_m satisfies the Nyquist stability criterion, the cascaded system will be stable. As mentioned earlier, in this paper, the DAB converter is current controlled and the AC-DC rectifier is voltage controlled. Furthermore, this control arrangement is independent of the power flow direction. Therefore, the impedance ratio T_m in the both power flow direction can be uniformly expressed as

$$T_m = \frac{Z_{out}}{Z_{in\_DAB}} \tag{14}$$

where Z_{out} and Z_{in_DAB} are shown in (11) and (13), respectively.

By substituting (11) and (13) into (14), T_m can be obtained. The bode plots of Z_{in_DAB} and Z_{out} are shown in Fig. 6. The circuit and controller parameters are listed in Table 1 in page 7. From Fig. 6, when the two-stage converter operates at the half load condition, there is no intersection of $|Z_{in\_DAB}|$ and $|Z_{out}|$, which indicates that the two-stage converter is stable. However, $|Z_{in\_DAB}|$ and $|Z_{out}|$ intersect with each other under full load condition and the intersection frequencies f_1 and f_2 are 48 Hz and 82 Hz, respectively. Since the phase difference between Z_{in_DAB} and Z_{out} is larger than 180° at f_1, the

TABLE 1. Specifications of the two-stage converter.

Symbol	Parameter	Value
R_b	Equivalent Load of Battery	25 Ω
n	The Turns Ratio of The Transformer	2
D_1	The Phase-Shift Ratio of The First H-Bridge	0.5
I_l	The Rated Inductor Current in The DAB Converter	28 A
C_b	The DC Side Output Filter Capacitance	800 μF
L	DC Inductor	0.001 H
K_p	Proportional Coefficient of The Current Controller for the DAB Converter	1
K_i	Integral Coefficient of the Current Controller for the DAB Converter	60
f_s	Switching Frequency of the DAB Converter	20 kHz
V_{dc}	DC Bus Voltage	660 V
C_{dc}	DC Bus Filter Capacitance	2,000 μF
K_{pv}	Proportional Coefficient of The DC Voltage Controller for the AC-DC rectifier	7.5
K_{iv}	Integral Coefficient of The DC Voltage Controller for the AC-DC rectifier	80
K_{pi}	Proportional Coefficient of the Current Controller for the AC-DC rectifier	4
K_{ii}	Integral Coefficient of the Current Controller for the AC-DC rectifier	100
L_g	Filter Inductor of the AC-DC rectifier	0.002 H

$$\begin{bmatrix}\dot{\hat{i}}_d\\ \dot{\hat{i}}_q\\ \dot{\hat{v}}_{dc}\end{bmatrix} = \begin{bmatrix}\frac{V_{dc}G_{acv}}{L_g} & \omega_1 & \frac{-D_d + V_{dc}G_{acv}G_{acv}}{L_g}\\ -\omega_1 & \frac{V_{dc}G_{acv}}{L_g} & -\frac{D_q}{L_g}\\ \frac{3D_d - 3I_dG_{acv}}{2C_{dc}} & \frac{3D_q - 3I_qG_{acv}}{2C_{dc}} & -\frac{3I_dG_{acv}G_{acv}}{2C_{dc}}\end{bmatrix}\begin{bmatrix}\hat{i}_d\\ \hat{i}_q\\ \hat{v}_{dc}\end{bmatrix} + \frac{1}{L_g}\begin{bmatrix}\hat{v}_{gd}\\ \hat{v}_{gq}\\ 0\end{bmatrix} + \frac{-1}{C_{dc}}\begin{bmatrix}0\\ 0\\ \hat{i}_o\end{bmatrix} \tag{12}$$

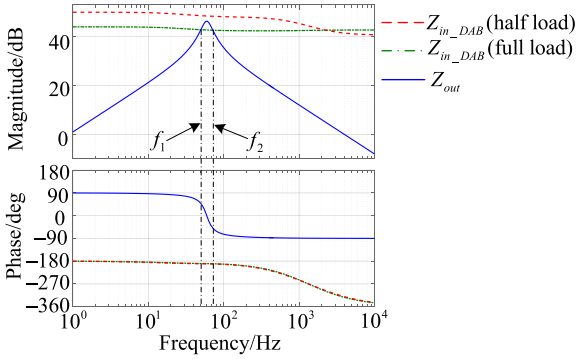

FIGURE 6. Bode plots of Z_{out} and Z_{in_DAB} under half or full load conditions in battery charging mode.

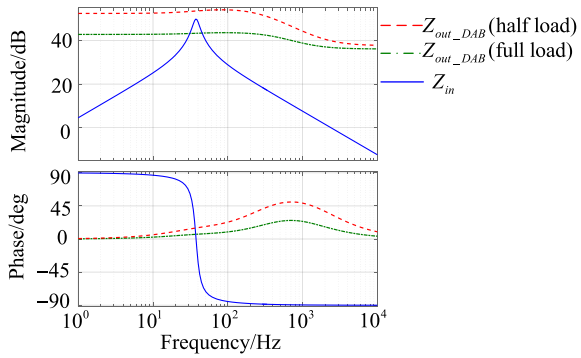

FIGURE 7. Bode plots of Z_{out} and Z_{in_DAB} under half or full load conditions in battery discharging mode.

two-stage converter is unstable and the oscillation frequency of the DC-link voltage should be the same as f_1.

For comparison purpose, the impedances of the two-stage converter in battery discharging mode are shown in Fig. 7. The output impedance of the DAB converter Z_{out_DAB} shows the positive resistance behavior at the low frequencies. So the two-stage converter is always stable in battery discharging mode, because the phase difference between the DAB output impedance and the rectifier input impedance is always smaller than 180°.

To solve the unstable problem in battery charging mode, a simple way is to increase the magnitude of the DAB converter input impedance. In other words, the magnitude of the DAB converter's input admittance should be reduced. On the other hand, it is worth noting that the impedance intersection occurs within the low frequencies (before the crossover frequency of the AC-DC rectifier). This can lead to the unstable operation of the two-stage converter. Therefore, it is important to modify the impedance characteristics of the DAB converter within the low frequency range to satisfy the stability criterion. This can be realized by introducing a feedforward or feedback path in the control loop, since the feedforward or feedback path can change either the numerator or the denominator of the impedance formulas, respectively. Based on these two ideas, two impedance shaping

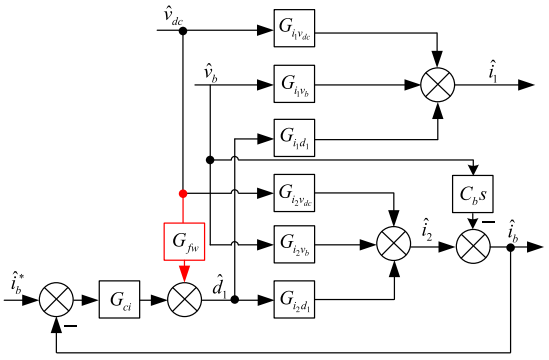

FIGURE 8. Control block of voltage feedforward loop of DAB converter.

control methods are proposed for the DC-link voltage stabilization in the following sections.

B. VOLTAGE FEEDFORWARD CONTROL

From the basic control block diagram shown in Fig. 5, there are two existing feedforward paths from $\hat{v}_{dc}$ to $\hat{i}_1$. The numerator of $\hat{Y}_{in\_DAB}$ can be reduced if one more negative feedforward path is added so that the magnitude of $\hat{Y}_{in\_DAB}$ will also be reduced.

As shown in Fig. 8, the additional voltage feedforward path is created. The feedforward controller is denoted by G_{fw}. The input admittance of the DAB converter with the voltage feedforward control can be expressed as

$$\begin{aligned} Y_{fw\_DAB} &= G_{i_1v_1} - \frac{G_{i_1d_1}G_{ci}G_{i_2v_1} + G_{fw}G_{i_1d_1}}{1 + G_{ci}G_{i_2d_1}} \\ &= Y_{in\_DAB} + Y_{vir\_fw} \end{aligned} \tag{15}$$

where $Y_{vir\_fw} = \frac{G_{fw}G_{i_1d_1}}{1+G_{ci}G_{i_2d_1}}$ is the virtual admittance connected in parallel with the Y_{in_DAB}.

Since the maximum value of Z_{out} occurs at the crossover frequency f_c, the characteristics of the impedances within the low frequency (below f_c) are of most interest. The objective is to reduce the magnitude of Y_{fw_DAB} within low frequencies. Hence, the impedance intersection in the two-stage converter can be avoided. As Y_{vir_fw} is connected in parallel with Y_{in_DAB}, Y_{vir_fw} should satisfy the following requirements:

$$\begin{cases} \left|Y_{vir\_fw} + Y_{in\_DAB}\right| < \left|Y_{in\_DAB}\right| (f < f_c) \\ \left|Y_{vir\_fw}\right| = 0 \, (f \geq f_c) \end{cases} \tag{16}$$

According to (16), Y_{vir_fw} is a piecewise function, which equals to zero within high frequencies (beyond f_c). Hence, a low-pass filter G_{LPF} is required to realize G_{fw}. In this paper, the typical one-order low-pass filter, shown in (17), is utilized.

$$G_{LPF} = \frac{A\omega_1}{s + \omega_1} \tag{17}$$

where $\omega_1 = 2\pi f_1$ is the characteristic angular frequency of the low-pass filter. A is the gain of the low-pass filter.

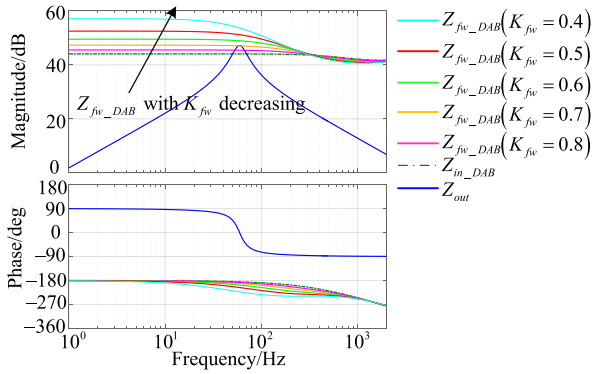

FIGURE 9. Bode plots of Z_{out}, Z_{in_DAB} and Z_{in_fw} under full load.

To replace the denominator of Y_{vir_fw}, G_{fw} can be expressed as:

$$G_{fw} = K_{fw}\left(1 + G_{ci}G_{i_2d_1}\right)G_{LPF} \tag{18}$$

where K_{fw} is the gain of the feedforward controller.

Then Y_{vir_fw} can be represented as:

$$\begin{cases} Y_{vir\_fw} = K_{fw}G_{i_1d_1}\ (f < f_c) \\ Y_{vir\_fw} = 0\ (f \geq f_c) \end{cases} \tag{19}$$

When f is smaller than f_c, the integral parameter of the DAB controller dominates over the proportional parameter. So, the original admittance of the DAB converter can be approximated as:

$$Y_{in\_DAB} \approx G_{i_1v_1} - \frac{G_{i_1d_1}}{G_{i_2d_1}}G_{i_2v_1} \tag{20}$$

Substituting (19) and (20) into (16), the coefficient K_{fw} should be confined within the range expressed in (21).

$$0 < K_{fw} < \frac{G_{i_2v_1}}{G_{i_2d}} - \frac{G_{i_1v_1}}{G_{i_1d}} \tag{21}$$

Fig. 9 shows the bode plots of the AC-DC rectifier output impedance Z_{out} and the DAB input impedances under the full load condition. Z_{in_DAB} and Z_{fw_DAB} denote the input impedance of the DAB converter with and without the proposed voltage feedforward control respectively. The coefficient K_{fw} is gradually decreased from 0.8 to 0.4 according to the constraint in (21). From Fig. 9, the magnitude of Z_{fw_DAB} increases within the low frequencies as K_{fw} decreases. And Z_{fw_DAB} becomes larger than Z_{out} when K_{fw} is less than 0.6. Moreover, within the low frequency range, the input impedance of the DAB converter Z_{fw_DAB} remains negative resistance characteristics. The characteristics of Z_{fw_DAB} also keep the same with Z_{in_DAB} at high frequencies. Therefore, the stability of the two-stage converter can be improved without affecting its dynamics by the proposed voltage feedforward control.

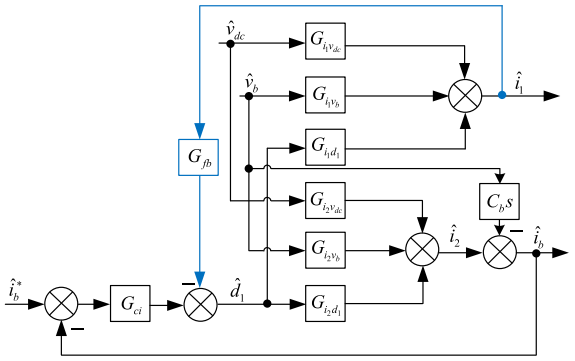

FIGURE 10. Control block of current feedback loop of DAB converter.

C. CURRENT FEEDBACK CONTROL

The impedance characteristics of the DAB converter can also be modified if the denominator of Z_{in_DAB} is reduced. This can be realized by adding a negative feedback control loop from $\hat{i}_1$ to $\hat{v}_{dc}$. Fig. 10 shows the current feedback control strategy. The feedback controller is denoted by G_{fb}. The input admittance of the DAB converter can be obtained by (22).

$$Y_{fb\_DAB} = \frac{G_{i_1v_1}\left(1 + G_{ci}G_{i_2d_1}\right) - G_{i_2v_1}G_{ci}G_{i_1d_1}}{1 + G_{ci}G_{i_2d_1} - G_{fb}G_{i_1d_1}} \tag{22}$$

It can be easily obtained that the input impedance of the DAB converter with the current feedback control can be expressed as:

$$\begin{aligned} Z_{fb\_DAB} &= \frac{1 + G_{ci}G_{i_2d_1} - G_{fb}G_{i_1d_1}}{G_{i_1v_1}\left(1 + G_{ci}G_{i_2d_1}\right) - G_{i_2v_1}G_{ci}G_{i_1d_1}} \\ &= Z_{in\_DAB} + Z_{vir\_fb} \end{aligned} \tag{23}$$

where $Z_{vir\_fb} = \frac{-G_{fb}G_{i_1d_1}}{G_{i_1v_1}(1+G_{ci}G_{i_2d_1})-G_{i_2v_1}G_{ci}G_{i_1d_1}}$ is the virtual impedance connected in series with the Z_{in_DAB}.

To avoid the impedance intersection of the two-stage converter, the magnitude of Z_{fb_DAB} should be increased at low frequencies (below f_c). Since Z_{vir_fb} is connected in series with Z_{in_DAB}, Z_{vir_fb} should satisfy the following requirement:

$$\begin{cases} \left|Z_{vir\_fb} + Z_{in\_DAB}\right| > \left|Z_{in\_DAB}\right| & (f < f_c) \\ \left|Z_{vir\_fb}\right| = 0 & (f \geq f_c) \end{cases} \tag{24}$$

According to (24), Z_{vir_fb} is a piecewise function, which equals to zero within high frequencies (beyond f_c). Similar to G_{fw}, the low-pass filter expressed in (17) is also applied in G_{fb}. Then G_{fb} can be expressed as:

$$G_{fb} = K_{fb}\left[G_{i_1v_1}\left(1 + G_{ci}G_{i_2d_1}\right) - G_{i_2v_1}G_{ci}G_{i_1d_1}\right]G_{LPF} \tag{25}$$

where K_{fb} is the coefficient of the current feedback controller.

Z_{vir_fb} is further simplified as (26).

$$\begin{cases} Z_{vir\_fb} = -K_{fb}G_{i_1d_1}\ (f < f_c) \\ Z_{vir\_fb} = 0\ (f \geq f_c) \end{cases} \tag{26}$$

The integral parameter of the controller dominates over the proportional parameter within low frequencies, the original

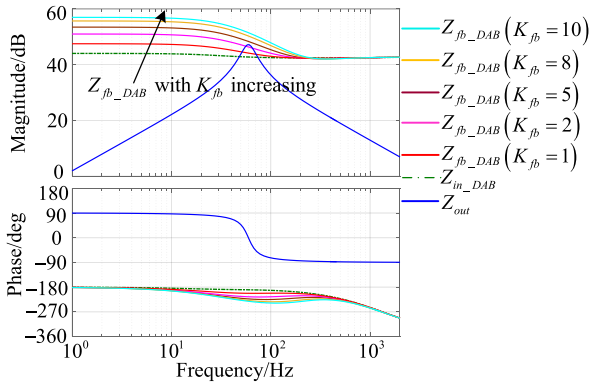

FIGURE 11. Bode plots of Z_{out}, Z_{in_DAB} and Z_{fb_DAB} under full load.

impedance of the DAB converter can be assumed as:

$$Z_{in\_DAB} \approx \frac{G_{i_2d_1}}{G_{i_2d_1}G_{i_1v_1} - G_{i_1d_1}G_{i_2v1}} \tag{27}$$

Substituting (26) and (27) into (24), the coefficient K_{fb} should satisfy the following requirement:

$$K_{fb} > 0 \tag{28}$$

Fig. 11 shows the bode plots of the AC-DC rectifier output impedance Z_{out} and the DAB impedances with/without the proposed current feedback control Z_{in_DAB} and Z_{fb_DAB} under the full load condition. From Fig. 11, the magnitude of Z_{fw_DAB} increases gradually with the increase of K_{fb}. And there is no intersection between the two impedances Z_{fb_DAB} and Z_{out} when K_{fb} is larger than 2. The phase of Z_{fb_DAB} keeps at $-180°$ within low frequencies and the characteristics of Z_{fb_DAB} are the same with Z_{in_DAB}. Therefore, the stability of the two-stage converter is enhanced with the proposed current feedback control.

D. COMPARISON OF TWO PROPOSED CONTROL METHODS

The objectives of the voltage feedforward control and the current feedback control are to improve the stability of the two-stage converter. Both of them can accomplish the goal by reshaping the input impedance of the DAB converter as shown in Fig. 9 and Fig. 11. The idea of the voltage feedforward control is to build a virtual impedance connected in parallel with the original DAB impedance, while the current feedback control adds a virtual impedance connected in series with the original DAB impedance.

It can be seen from Fig. 8 and Fig. 10 that the ratio of the battery current $\hat{i}_b$ to the reference current $\hat{i}_b^*$ can be uniformly expressed as:

$$\frac{\hat{i}_b}{\hat{i}_b^*} = \frac{G_{ci}G_{i_2d_1}}{1 + G_{ci}G_{i_2d_1}} \tag{29}$$

It means the dynamic responses of the current controller are not affected by these two control methods. In addition, the proposed two control methods are to reshape the input impedance of the DAB converter and the control schemes of the DAB converter and the AC-DC rectifier are independently implemented. So, the dynamics of the AC-DC rectifier will not be affected.

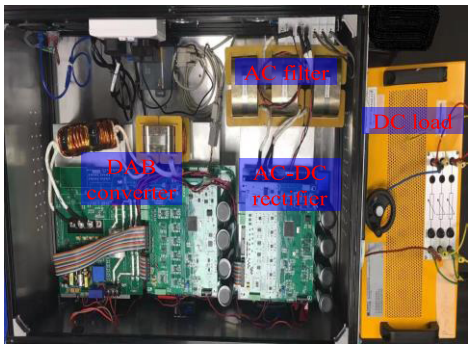

FIGURE 12. Prototype of the two-stage converter.

The difference between these two control methods is that the current feedback control requires an additional current sensor to measure the input current of the DAB converter. On the other hand, the voltage feedforward control regards the DC-link voltage as the controlled variable, which is already measured in the control loop of the AC-DC rectifier. Therefore, there is no additional voltage sensor needed. As a result, the cost of the voltage feedforward control is lower than that of the current feedback control. And the reliability of the voltage feedforward control is also higher than that of the current feedback control.

To sum up, although the stabilizing ability and the dynamic performance of these two control methods are the same, the voltage feedforward control is preferred as it requires fewer components.

IV. EXPERIMENTAL VERIFICATION AND DISCUSSION

The hardware prototype shown in Fig. 12 is built to validate the proposed two impedance shaping methods. The two-stage converter is controlled by the TMS320F28335 digital signal processor (DSP). As the power is transferred from the grid to the DC side, the battery can be replaced by the equivalent DC load. The circuit and controller parameters of the two-stage converter are listed in Table I.

The experimental results of the two-stage converter in battery charging mode without the proposed control methods are shown in Fig. 13. It should be noted that all the waveforms of V_{dc} measured in the experiments are only AC components to show the oscillation clearly. When the two-stage converter works at the half load, i.e. I_b is 5 A and V_b is 300 V, there is no oscillation in the DC-link voltage, which is as expected since there is no intersection between Z_{in_DAB} and Z_{out}. When I_b is increased to 10 A, which indicates that the two-stage converter works at the full load, severe oscillation in the DC-link voltage can be found as shown in Fig. 13(b). It is because the magnitude of Z_{in_DAB} becomes smaller when the total transferred power increases, especially within the low frequency range. As a result, Z_{in_DAB} and Z_{out} intersect

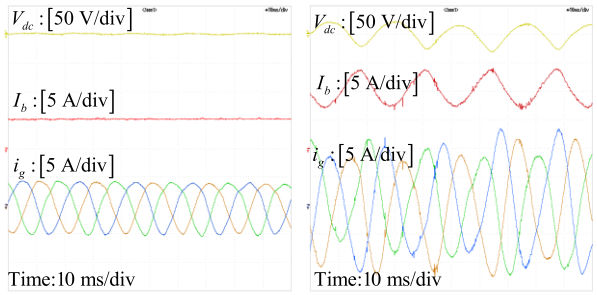

FIGURE 13. Waveforms of V_{dc}, I_b, V_b and grid current i_g in battery charging mode without proposed control under (a) half load; and (b) full load.

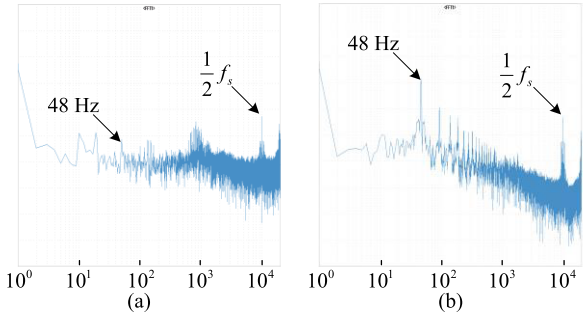

FIGURE 14. FFT analysis of V_{dc} in battery charging mode without proposed control under (a) half load; and (b) full load.

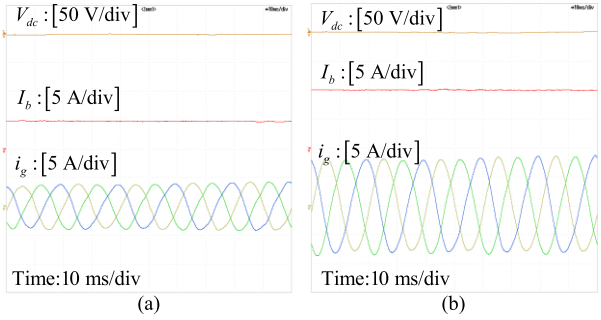

FIGURE 15. Waveforms of V_{dc}, I_b, V_b and grid current i_g in battery discharging mode without proposed control under (a) half load; and (b) full load.

each other between 48 Hz and 82 Hz, as shown in Fig. 6. The experimental results also validate the theoretical analysis as the oscillating frequency of the DC-link voltage is around 48 Hz. The stability of the two-stage converter can be more visualized from the FFT spectra of the V_{dc} shown in Fig. 14. In comparison to the case of the half load operation, the amplitude of the 48 Hz harmonic component increases significantly when the two-stage converter operates at full load condition. This measured trend is in close agreement with the waveform oscillation shown in Fig. 14(b).

The waveforms of the two-stage converter in battery discharging mode are shown in Fig. 15. From the experimental waveforms, the two-stage converter in battery discharging

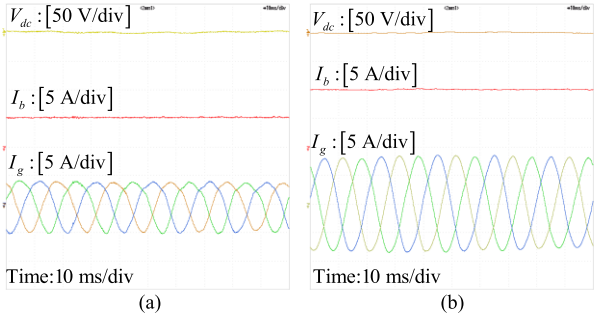

FIGURE 16. Waveforms of V_{dc}, I_b, V_b and grid current i_g with voltage feedforward control under (a) half load; and (b) full load.

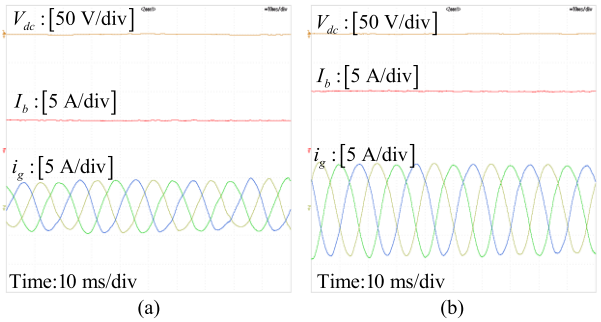

FIGURE 17. Waveforms of V_{dc}, I_b, V_b and grid current i_g with current feedback control under (a) half load; and (b) full load.

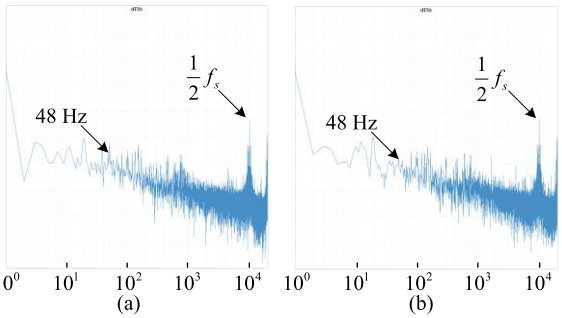

FIGURE 18. FFT analysis of V_{dc} under full load with proposed methods under (a) voltage feedforward control; and (b) current feedback control.

mode is stable even in full load condition, which corresponds to the analysis in Fig. 7. Therefore, no additional control loop is required to improve the stability of the two-stage converter in battery discharging mode.

Fig. 16 shows the experimental results of the two-stage converter with the proposed voltage feedforward control method implemented. The waveforms of the two-stage converter remain stable even in the full load condition. This means the impedance characteristic of the DAB converter is successfully reshaped and the stability criterion is satisfied. Similar results can be obtained from Fig. 17 when the current feedback control is realized. The oscillation in the DC-link is mitigated even in the full load condition, which shows the effectiveness of the proposed current feedback control method. The FFT analysis of V_{dc} under full load operation

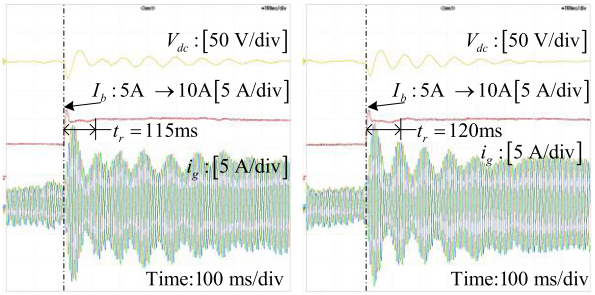

FIGURE 19. Waveforms of V_{dc}, I_b, V_b and grid current i_g under a load step change with the proposed control methods. (a) voltage feedforward control; and (b) current feedback control.

is shown in Fig. 18. The quantities of the harmonic response are suppressed when the proposed two control methods are implemented. The results validate the effectiveness of the proposed control methods.

Fig. 19 shows the dynamic performance of the two-stage converter with the proposed voltage feedforward control and current feedback control, respectively. The proposed voltage feedforward control and current feedback control can both stabilize the waveforms of the DC-link voltage and the grid current when I_b steps from 5 A to 10 A. I_b has also become stable after a short overshoot and the transient period t_r with voltage feedforward control is 115 ms, while t_r is 120 ms with current feedback control. Since the proposed two control methods are both aimed at the DAB converter, the dynamics of the AC-DC rectifier is not affected.

V. CONCLUSION

In this paper, the small signal impedance models of the DAB converter and the AC-DC rectifier of the two-stage converter are derived for the stability analysis. To improve the stability of the two-stage converter, two impedance shaping methods are proposed by adding a parallel or series connected virtual impedance. The input impedance of the DAB is modified to satisfy the stability criterion. The controller parameter design rules of these two methods are provided to ensure the stable operation of the two-stage converter. Furthermore, the comparison of these two control methods is discussed and the voltage feedforward-based impedance shaping method is preferred because of the less of cost. Comprehensive steady-state and dynamic experimental results of the two-stage converter validate the effectiveness of the proposed methods. The proposed methods are useful for stabilizing the two-stage AC-DC-DC converter and can also be extended for other cascaded applications to improve the stability margin.

REFERENCES

[1] F. Blaabjerg, A. Consoli, J. A. Ferreira, and J. D. V. Wyk, "The future of electronic power processing and conversion," *IEEE Trans. Power Electron.*, vol. 20, no. 3, pp. 715–720, May 2005.

[2] S. Luo, "A review of distributed power systems part I: DC distributed power system," *IEEE Aerosp. Electron. Syst. Mag.*, vol. 20, no. 8, pp. 5–16, Aug. 2005.

[3] F. Blaabjerg, Z. Chen, and S. B. Kjaer, "Power electronics as efficient interface in dispersed power generation systems," *IEEE Trans. Power Electron.*, vol. 19, no. 5, pp. 1184–1194, Sep. 2004.

[4] P. Wang, X. Lu, W. Wang, and D. Xu, "Frequency division based coordinated control of three-port converter interfaced hybrid energy storage systems in autonomous DC microgrids," *IEEE Access*, vol. 6, pp. 25389–25398, 2018.

[5] B. Zhao, S. Qiang, W. Liu, and Y. Sun, "Overview of dual-active-bridge isolated bidirectional DC-DC converter for high-frequency-link power-conversion system," *IEEE Trans. Power Electron.*, vol. 29, no. 8, pp. 4091–4106, Aug. 2014.

[6] A. R. Alonso, J. Sebastian, D. G. Lamar, M. M. Hernando, and A. Vazquez, "An overall study of a dual active bridge for bidirectional DC/DC conversion," in *Proc. IEEE Energy Convers. Congr. Expo. (ECCE)*, Sep. 2010, pp. 1129–1135.

[7] H. Krishnamurthy and R. Ayyanar, "Stability analysis of cascaded converters for bidirectional power flow applications," in *Proc. IEEE 30th Int. Telecommun. Energy Conf. (INTELEC)*, Sep. 2008, pp. 1–8.

[8] M. Khazraei, V. A. K. Prabhala, R. Ahmadi, and M. Ferdowsi, "Solid-state transformer stability and control considerations," in *Proc. 29th Annu. Appl. Power Electron. Conf. Expo. (APEC)*, Mar. 2014, pp. 2237–2244.

[9] Y. Tian, P. C. Loh, Z. Chen, F. Deng, and Y. Hu, "Impedance interactions in bidirectional cascaded converter," *IET Power Electron.*, vol. 9, no. 13, pp. 2482–2491, Oct. 2016.

[10] R. D. Middlebrook and S. Cuk, "A general unified approach to modelling switching-converter power stages," in *Proc. IEEE Power Electron. Spec. Conf.*, Jun. 1976, pp. 18–34.

[11] J. Sun, "Impedance-based stability criterion for grid-connected inverters," *IEEE Trans. Power Electron.*, vol. 26, no. 11, pp. 3075–3078, Nov. 2011.

[12] X. Zhang, X. Ruan, and C. K. Tse, "Impedance-based local stability criterion for DC distributed power systems," *IEEE Trans. Circuits Syst. I, Reg. Papers*, vol. 62, no. 3, pp. 916–925, Mar. 2015.

[13] M. Cespedes, L. Xing, and J. Sun, "Constant-power load system stabilization by passive damping," *IEEE Trans. Power Electron.*, vol. 26, no. 7, pp. 1832–1836, Jul. 2011.

[14] Y. A.-R. I. Mohamed, A. A. A. Radwan, and T. K. Lee, "Decoupled reference-voltage-based active DC-link stabilization for PMSM drives with tight-speed regulation," *IEEE Trans. Ind. Electron.*, vol. 59, no. 12, pp. 4523–4536, Dec. 2012.

[15] S. S. Kelkar and F. C. Lee, "Stability analysis of a buck regulator employing input filter compensation," in *Proc. IEEE Power Electron. Spec. Conf.*, Jun. 1983, pp. 38–49.

[16] W.-J. Lee and S.-K. Sul, "DC-link voltage stabilization for reduced DC-link capacitor inverter," *IEEE Trans. Ind. Appl.*, vol. 50, no. 1, pp. 404–414, Jan./Feb. 2014.

[17] R. Haroun, A. Cid-Pastor, A. El Aroudi, and L. Martinez-Salamero, "Synthesis of canonical elements for power processing in dc distribution systems using cascaded converters and sliding-mode control," *IEEE Trans. Power Electron.*, vol. 29, no. 3, pp. 1366–1381, Mar. 2014.

[18] L. Cao, K. H. Loo, and Y. M. Lai, "Systematic derivation of a family of output-impedance shaping methods for power converters—A case study using fuel cell-battery-powered single-phase inverter system," *IEEE Trans. Power Electron.*, vol. 30, no. 10, pp. 5854–5869, Oct. 2015.

[19] A. Khaligh, A. M. Rahimi, and A. Emadi, "Modified pulse-adjustment technique to control DC/DC converters driving variable constant-power loads," *IEEE Trans. Ind. Electron.*, vol. 55, no. 3, pp. 1133–1146, Mar. 2008.

[20] A. M. Rahimi and A. Emadi, "Active damping in DC/DC power electronic converters: A novel method to overcome the problems of constant power loads," *IEEE Trans. Ind. Electron.*, vol. 56, no. 5, pp. 1428–1439, May 2009.

[21] W. W. Weaver and P. T. Krein, "Optimal geometric control of power buffers," *IEEE Trans. Power Electron.*, vol. 24, no. 5, pp. 1248–1258, May 2009.

[22] X. Zhang, D. M. Vilathgamuwa, K. J. Tseng, B. S. Bhangu, and C. J. Gajanayake, "Power buffer with model predictive control for stability of vehicular power systems with constant power loads," *IEEE Trans. Power Electron.*, vol. 28, no. 12, pp. 5804–5812, Dec. 2013.

[23] Y. Huangfu, S. Pang, B. Nahid-Mobarakeh, L. Guo, A. K. Rathore, and F. Gao, "Stability analysis and active stabilization of on-board DC power converter system with input filter," *IEEE Trans. Ind. Electron.*, vol. 65, no. 1, pp. 790–799, Jan. 2018.

[24] J. Wang and D. Howe, "A power shaping stabilizing control strategy for DC power systems with constant power loads," *IEEE Trans. Power Electron.*, vol. 23, no. 6, pp. 2982–2989, Nov. 2008.

[25] P. Magne, B. Nahid-Mobarakeh, and S. Pierfederici, "Dynamic consideration of DC microgrids with constant power loads and active damping system—A design method for fault-tolerant stabilizing system," *IEEE J. Emerg. Sel. Topics Power Electron.*, vol. 2, no. 3, pp. 562–570, Sep. 2014.
[26] S. D. Sudhoff, K. A. Corzine, S. F. Glover, H. J. Hegner, and H. N. Robey, Jr., "DC link stabilized field oriented control of electric propulsion systems," *IEEE Trans. Energy Convers.*, vol. 13, no. 1, pp. 27–33, Mar. 1998.
[27] P. Liutanakul, A. B. Awan, S. Pierfederici, B. Nahid-Mobarakeh, and F. Meibody-Tabar, "Linear stabilization of a DC bus supplying a constant power load: A general design approach," *IEEE Trans. Power Electron.*, vol. 25, no. 2, pp. 475–488, Feb. 2010.
[28] X. Y. Liu and A. J. Forsyth, "Comparative study of stabilizing controllers for brushless DC motor drive systems," in *Proc. IEEE Int. Conf. Electr. Mach. Drives*, May 2005, pp. 1725–1731.
[29] M. Wu and D. D.-C. Lu, "A novel stabilization method of LC input filter with constant power loads without load performance compromise in DC microgrids," *IEEE Trans. Ind. Electron.*, vol. 62, no. 7, pp. 4552–4562, Jul. 2015.
[30] X. Zhang, Q.-C. Zhong, V. Kadirkamanathan, J. He, and J. Huang, "Source-side series-virtual-impedance control to improve the cascaded system stability and the dynamic performance of its source converter," *IEEE Trans. Power Electron.*, to be published, doi: 10.1109/TPEL.2018.2867272.
[31] N. Mohan, *Power Electronics: Converters Applications and Design*. Hoboken, NJ, USA: Wiley, 2003.
[32] F. Wu, F. Feng, and H. B. Gooi, "Analysis of dual-side reactive currents of isolated DAB DC-DC converter and elimination strategy," in *Proc. IEEE 3rd Int. Future Energy Electron. Conf. ECCE Asia (ECCE Asia)*, Jun. 2017, pp. 1812–1816.
[33] F. Wu, F. Feng, and H. B. Gooi, "Cooperative triple-phase-shift control for isolated dab converter to improve current characteristics," *IEEE Trans. Ind. Electron.*, to be published, doi: 10.1109/TIE.2018.2877115.
[34] Y. Zhao and T. A. Lipo, "Space vector PWM control of dual three-phase induction machine using vector space decomposition," *IEEE Trans. Ind. Appl.*, vol. 31, no. 5, pp. 1100–1109, Sep. 1995.

FAN FENG received the B.S. and M.S. degrees in electrical engineering from the Harbin Institute of Technology, Harbin, China, in 2011 and 2015, respectively. He is currently pursuing the Ph.D. degree with the School of Electrical and Electronic Engineering, Nanyang Technological University, Singapore.

His research interests include power electronic system stability analysis and active stabilization methods.

FENGJIANG WU (M'15–SM'17) received the B.S., M.S., and Ph.D. degrees in electrical engineering from the Harbin Institute of Technology (HIT), Harbin, China, in 2002, 2004, and 2007, respectively.

Since 2007, he has been with the Department of Electrical Engineering, HIT, where he is currently an Associate Professor.

From 2016 to 2017, he was a Senior Research Fellow with Nanyang Technological University, Singapore. He has published more than 30 top-tier journal papers. His research interests include the areas of renewable energy generation, solid-state transformer, microgrid, multilevel inverter technology, and electric machines drives. He serves as an Associate Editor for the IEEE Access and *IET Power Electronics*.

HOAY BENG GOOI (SM'95) received the B.S. degree in electrical engineering from National Taiwan University, Taipei, Taiwan, in 1978, the M.S. degree in power engineering from the University of New Brunswick, Fredericton, NB, Canada, in 1980, and the Ph.D. degree in power engineering from Ohio State University, Columbus, OH, USA, in 1983.

From 1983 to 1985, he was an Assistant Professor with the Department of Electrical Engineering, Lafayette College, Easton, PA, USA. From 1985 to 1991, he was a Senior Engineer with Empros (Siemens), Minneapolis, MN, USA, where he was responsible for the design and testing coordination of the domestic and international energy management system projects. In 1991, he joined the School of Electrical and Electronic Engineering, Nanyang Technological University, Singapore, as a Senior Lecturer, where he has been an Associate Professor, since 1999, and the Deputy Head of the Power Engineering Division, from 2008 to 2014. His current research interests include microgrid energy management systems, electricity markets, spinning reserve, energy storage, and renewable energy sources.